Svenningsen, L., Balling, N., Jacobsen, B. H., Kind, R., Wylegalla, K., Schweitzer, J. (2007): Crustal root beneath the highlands of southern Norway resolved by teleseismic receiver functions. - Geophysical Journal International, 170, 3, pp. 11129—1138.

DOI: http://doi.org/10.1111/j.1365-246X.2007.03402.x

Geophys. J. Int. (2007) **170,** 1129–1138 doi: 10.1111/j.1365-246X.2007.03402.x

Crustal root beneath the highlands of southern Norway resolved by teleseismic receiver functions

L. Svenningsen,[1] N. Balling,[1] B. H. Jacobsen,[1] R. Kind,[2] K. Wylegalla[2] and J. Schweitzer[3]

[1] *Department of Earth Sciences, University of Aarhus, Høegh-Guldbergs Gade* 2, 8000 *Aarhus C, Denmark. E-mail: lasse.svenningsen@geo.au.dk*
[2] *GeoForschungsZentrum Potsdam, Telegrafenberg,* 1447 *Potsdam, Germany*
[3] *NORSAR, Instituttveien* 25, 2007 *Kjeller, Norway*

Accepted 2007 February 13. Received 2007 February 12; in original form 2006 June 29

SUMMARY

Teleseismic data have been collected with temporary seismograph stations on two profiles in southern Norway. Including the permanent arrays NORSAR and Hagfors the profiles are 400 and 500 km long and extend from the Atlantic coast across regions of high topography and the Oslo Rift. A total of 1071 teleseismic waveforms recorded by 24 temporary and 8 permanent stations are analysed. The depth-migrated receiver functions show a well-resolved Moho for both profiles with Moho depths that are generally accurate within ±2 km.

For the northern profile across Jotunheimen we obtain Moho depths between 32 and 43 km (below sea level). On the southern profile across Hardangervidda, the Moho depths range from 29 km at the Atlantic coast to 41 km below the highland plateau. Generally the depth of Moho is close to or above 40 km beneath areas of high mean topography (>1 km), whereas in the Oslo Rift the crust locally thins down to 32 km. At the east end of the profiles we observe a deepening Moho beneath low topography. Beneath the highlands the obtained Moho depths are 4–5 km deeper than previous estimates. Our results are supported by the fact that west of the Oslo Rift a deep Moho correlates very well with low Bouguer gravity which also correlates well with high mean topography.

The presented results reveal a *ca*. 10–12 km thick Airy-type crustal root beneath the highlands of southern Norway, which leaves little room for additional buoyancy-effects below Moho. These observations do not seem consistent with the mechanisms of substantial buoyancy presently suggested to explain a significant Cenozoic uplift widely believed to be the cause of the high topography in present-day southern Norway.

Key words: crustal root, Moho discontinuity, receiver function, southern Norway, topography, uplift.

1 INTRODUCTION

The western part of the Scandinavian peninsula is widely believed to have experienced a significant uplift in the Cenozoic era (e.g. Doré 1992; Stuevold & Eldholm 1996; Japsen & Chalmers 2000; Lidmar-Bergström *et al.* 2000). It is suggested that the current relief has risen from a peneplane since the end of Cretaceous. Timing as well as possible mechanisms behind this uplift are, however, debated (Rohrman & van der Beek 1996; Nielsen *et al.* 2002; Gabrielsen *et al.* 2005). The presented suggestions include asthenospheric diapirism (Rohrman & van der Beek 1996), lithospheric delamination and magmatic underplating (Nielsen *et al.* 2002). This study contributes to the solution of these problems by presenting new geophysical information on the crustal structure beneath regions of high topography in southern Norway.

We study the crustal structure beneath southern Norway with teleseismic data collected along two profiles: a northern profile from Ålesund in the west through Hamar to Hagfors in the east and a southern profile from Bergen in the west to Hamar in the east (see Fig. 1). The northern profile was conducted between 2002 May and 2004 March with up to 11 temporary seismograph stations installed simultaneously. Station spacing was around 25 km. This profile crossed Jotunheimen, the area in Scandinavia of maximum topography. The southern profile across Hardangervidda was conducted between 2005 April and December and included 15 stations. Station spacing along the profile line was around 25 km, with two stations placed about 50 km north of this line in order to facilitate future surface wave studies. To supplement the temporary stations of this study we also include data from three-component seismograph stations in the permanent arrays NORSAR (Norway) and Hagfors

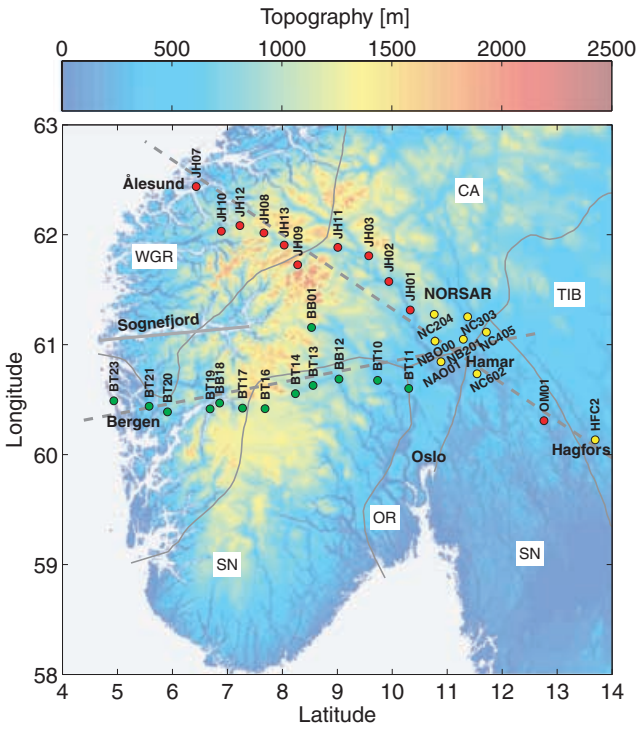

Figure 1. The topography of southern Norway with positions and names of the temporary seismograph stations on the southern profile across Hardangervidda (green) and the northern profile across Jotunheimen (red), and of the permanent seismograph stations included in this study (yellow). The two dashed lines are those used to generate the depth migrated cross-sections. Also outlined are the main tectonic units in southern Norway: Sweconorwegian Orogen (SN), Western Gneiss Region (WGR), Caledonian Allochtons (CA), Oslo Rift (OR) and Transscandinavian Igneous Belt (TIB). (mainly after Gaál & Gorbatschev 1987).

(Sweden). With these permanent stations included, the two profiles span distances of 400 and 500 km, respectively. Positions and names of the seismograph stations are shown in Fig. 1 together with the topography and the main tectonic units of southern Norway.

Receiver function analysis of teleseismic data is a well-established way to study the depth of Moho and crustal structures, for example, Langston (1979), Owens *et al.* (1987), Kind *et al.* (1995), Gossler *et al.* (1999), Zhu & Kanamori (2000), Bostock *et al.* (2002), Dahl-Jensen *et al.* (2003) and Al-Damegh *et al.* (2005). The installation of temporary seismograph stations is quite simple and makes teleseismic investigations very well suited for the relatively inaccessible regions of the mountainous western Norway. An additional advantage is the generally low cost of teleseismic experiments in comparison to crustal scale controlled source experiments.

The crustal structure was previously studied in areas adjacent to both our teleseismic profiles. Early refraction seismic experiments (Kanestrøm & Haugland 1971; Sellevoll & Warrick 1971; Kanestrøm & Nedland 1975; Mykkeltveit 1980) outlined general *P*-wave velocity models for the crust and uppermost mantle and indicated an increase of Moho depths from coastal areas to the central parts of southern Norway. Kinck *et al.* (1993) presented a map of Moho depths for the Fennoscandian region based mainly upon these early refraction studies. For southern Norway this map shows depths to Moho around 30–32 km in coastal areas and up to about 38 km in the central areas. So far no controlled source experiments have been carried out in the areas of high topography covered by the two passive source profiles of this study.

More recently an OBS (ocean-bottom seismometer) wide-angle seismic experiment was carried out along the Sognefjord, which penetrates deep inland (Iwasaki *et al.* 1994). The studied region lies between the western parts of our two profiles (see Fig. 1), and both clear *P* and clear *S* arrivals were observed. The *P* velocity (V_P) and Poisson's ratio (σ) model of the crust that we apply in the depth migration of the receiver function estimates (Sections 4 and 5) is based mainly on the results of their study.

Ottemöller & Midzi (2003) presented Moho depth estimates based on single-station 1-D-receiver function inversion for permanent seismographs, primarily short-period stations along the Norwegian west coast. For southern Norway they obtained Moho depths ranging from 30 to 32 km for the southernmost part of the west coast to 38–40 km for the west coast just north of Ålesund (see Fig. 1).

Balling (1980, 1984) and Ebbing & Olesen (2005) have demonstrated a general close correlation between Bouguer gravity anomalies and surface elevation along the Scandinavian mountain range; areas of high surface elevation correlate well with areas of regional gravity lows. This is, in particular, also the case for southern Norway. The early seismic studies in southern Norway indicated a moderate crustal root below areas of elevated topography (e.g. Kanestrøm & Haugland 1971; Sellevoll & Warrick 1971) and thus argued for Airy-type isostasy. However, the existence of a conventional crustal root has been questioned, partly due to the lack of modern high quality seismological studies.

A main purpose of this study is to localize the crust–mantle boundary and to investigate whether a crustal root exists beneath the areas of high topography and the areas of low Bouguer gravity in southern Norway. In addition, we investigate whether other significant seismic boundaries exist in the lower crust and uppermost mantle. Such boundaries may be important for understanding the present state of isostasy and thus alternative explanations for the tectonic origin of the present relief of the Scandinavian mountains.

2 TECTONIC SETTING

The near-surface geology and the deep crustal structures of the area of investigation are formed through several tectonic events. Two main structural provinces are present: the Sveconorwegian province of the Precambrian Baltic shield and the Scandinavian Caledonides (Fig. 1).

The Baltic shield was formed through several tectonic accretional events with the oldest Archean units in the northeast and a generally decreasing structural age towards our study area in the southwest (Windley 1992; Gorbatschev & Bogdanova 1993; Balling 2000). The Sveconorwegian orogenic event (1.2–0.9 Ga) is the youngest Precambrian tectonic event of regional coverage. This collisional event largely reworked existing continental crust of Gothian age (*ca*. 1.7–1.5 Ga), which originally covered most of southwestern Scandinavia. Also present in the eastern part of the study area (see Fig. 1) is the Transscandinavian Igneous Belt (1.84–1.65 Ga). The westernmost part of this belt was also reworked by the Sveconorwegian orogeny.

The Scandinavian Caledonides were formed about 440–410 Ma ago as a result of continent–continent collision between Baltica and Laurentia following the closure of the Iapetus ocean (e.g. Torsvik 1998; Torsvik & Cocks 2005). Caledonian rocks are believed to form nappe structures underlain by Precambrian units of Baltica which are locally exposed within the Caledonian Allochtons (Gee & Sturt 1985; Gorbatschev & Bogdanova 1993; Roberts 2003). An area along the west coast of southern Norway is referred to as the

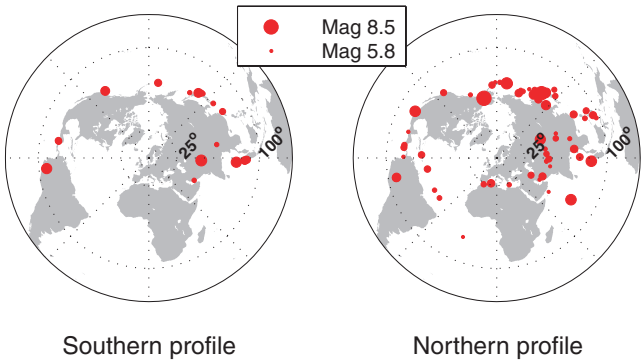

Figure 2. Positions of teleseismic events accepted for processing for the southern profile (Hardangervidda) and the northern profile (Jotunheimen), respectively.

Western Gneiss Region (see WGR in Fig. 1). WGR is assumed to be Precambrian Baltica crust previously covered by Caledonian Allochtons.

The youngest and yet significant tectonic event to affect southern Norway was the Permian rifting (*ca*. 305–245 Ma) which formed the Oslo Rift/Graben. This partial rifting resulted in both extrusives and intrusives and significantly thinned the crust in the Oslo region (e.g. Kinck *et al.* 1993).

3 INSTRUMENTATION AND DATA

The temporary seismograph stations were installed in cellars, garages or barns of local Norwegians living some distance from major roads, railways and other sources of noise. The equipment for the temporary stations on both profiles was supplied by the GFZ-Potsdam instrument pool. All recorded data are, therefore, stored in the GEOFON archive at GFZ-Potsdam.

On the the northern profile the seismometers were either broad-band (120 s) Streckeisen STS-2, intermediate-period (30 s) Güralp 40T or short-period (1 s) Mark L4, all equipped with REFTEK data loggers. These stations were operated at a sample frequency of 20 Hz. On the southern profile the seismometers were either Streckeisen STS-2 or Güralp 40T. All data loggers were Earth Data data loggers operated at 100 Hz. For use in this study data were resampled to 20 Hz.

From the raw data records we extract teleseismic events with distances from 25° to 100° and magnitudes above 5.7. Each event is then visually inspected and accepted for further processing if the arrival of the *P* wave is clear on both the vertical and either of the horizontal components. Only a few events below magnitude 6.0 passed this criterion.

Fig. 2 shows the position of the events which were accepted for processing on at least one station of the two profiles. Station information on elevation, recording equipment and the number of accepted events is summarized in Table 1.

The number of events accepted for further processing varies considerably from station to station. In several cases, for the northern profile of almost 2 yr duration, low numbers indicate that the station was moved to another site during the project. Other possible explanations include drift of calibration for the broad-band stations or a too high background noise. For the stations on the southern profile, the number of accepted events is generally lower than for the northern profile. This is a consequence of the much shorter deployment time and thus higher vulnerability to the problems mentioned above. Unfortunately, we had to omit two stations on the southern profile (BB02 and BB15) because no events were of acceptable quality.

4 METHOD

4.1 Estimation of receiver functions

Receiver functions can be estimated from recordings of teleseismic events in several different ways, for example, Langston (1979), Kind *et al.* (1995) and Bostock (1998). In this study we apply an estimation technique for *P*-to-*S* receiver functions similar to that of Kind *et al.* (1995). We remove the mean and the trend of the extracted events which are then filtered using an Ormsby bandpass filter with corner frequencies: (0.10, 0.15, 4.50 and 5.50) Hz. Backazimuths and apparent incidence angles are estimated by covariance analysis of the first few seconds after *P* onset. The estimates are used if they agree within 15° and 10° of the predicted angles using spherical geometry (backazimuth) and the global reference model IASP91 (apparent incidence angle; Kennett & Engdahl 1991). Otherwise the predicted values are used.

The backazimuths and apparent incidence angles are used in the LQT-rotation (Vinnik 1977) to approximately isolate the converted *SV* phases. In theory, this transformation entirely isolates the *P*

Table 1. Station names, elevations (h), instrument types and the number of teleseismic events (N_{ev}) accepted for receiver function estimation subject to the criteria described in the main text. BB, IP and SP denote broadband (120 s), intermediate-period (30 s) and short-period (1 s) instrument, respectively, and for instance BB/SP denotes that more than one instrument type has been installed, however, not simultaneously.

Jotunheimen				Hardangervidda				NORSAR/HAGFORS			
Name	h (m)	Inst.	N_{ev}	Name	h (m)	Inst.	N_{ev}	Name	h (m)	Inst.	N_{ev}
JH01	515	BB/SP	61	BB01	489	BB	8	NAO01	426	BB	80
JH02	393	SP	61	BB12	336	BB	12	NB201	613	BB	79
JH03	698	BB	49	BB18	135	BB	5	NBO00	529	BB	76
JH07	130	SP/IP	22	BT10	240	IP	11	NC204	851	BB	88
JH08	930	BB/SP	44	BT11	999	IP	19	NC303	401	BB	77
JH09	780	BB	4	BT13	493	IP	12	NC405	496	BB	80
JH10	198	SP/IP	28	BT14	904	IP	17	NC602	305	BB	41
JH11	490	SP/IP	9	BT16	1149	IP	1	HFC2	297	BB	43
JH12	401	BB/SP	25	BT17	721	IP	17				
JH13	527	BB/SP	29	BT19	34	IP	12				
OM01	123	SP	34	BT20	396	IP	5				
				BT21	122	IP	10				
				BT23	32	IP	12				

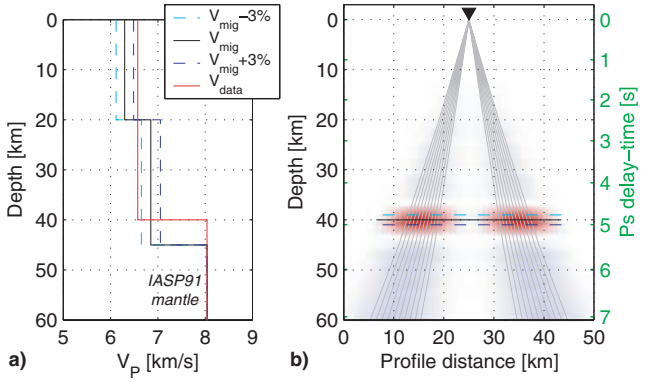

Figure 3. Synthetic example of the depth migration to illustrate the sensitivity of Moho depth to 3 per cent uncertainty in the V_P migration model. Rays traced using V_{mig} are shown in grey and the migrated *Ps*-phases of the synthetic data define a red zone (positive amplitude) centred at the full black line perfectly recovering the Moho depth of V_P (40 km). Moho depths obtained using the two 3 per cent perturbed V_P models are shown as dashed lines. Note the green scale of *Ps* delay-times on the right-hand side of (b) which corresponds to the depth scale on the left-hand side using V_{mig} and a reference slowness of 6.4 s deg^{-1}. For realistic appearance of the migration image, the synthetic *SV*-responses are convolved with the average of the deconvolved L-components for station JH03.

displacement on the L-component and the *SH* displacement on T, whereas the *SV* displacement is approximately isolated on the Q-component (Svenningsen & Jacobsen 2004).

Each Q-component is then deconvolved using a time-domain least-squares delayed spike (or spiking) filter estimated from the corresponding L-component (Petersen *et al.* 1993). In this way the source signature and the far path effects are neutralized, resulting in the receiver function estimates.

4.2 Depth migration

We depth migrate the receiver function estimates for each station using a simple ray migration procedure similar to that of Kosarev *et al.* (1999), also referred to as common conversion-point (CCP) stack. Each estimate is traced back along its ray using an *a priori* velocity model and then projected onto the profile plane to form a cross-section (see Fig. 3). The amplitudes are binned in a regular spatial grid (profile distance versus depth), and amplitudes from rays crossing the same bin are averaged. Laterally, the amplitude assigned to each bin is distributed to adjacent bins according to the width and weights determined by the first Fresnel zone for an assumed dominating frequency of 1 Hz. A correction for the elevation of each station (see Table 1) is applied in the depth migration to make the obtained depths relative to sea level.

In the depth migration an *a priori* velocity model must be assumed. For the *Ps*-conversion from Moho to migrate to the correct depth only the crustal averages of V_P and V_S or equivalently σ (Poisson's ratio) are important. However, for intra crustal conversions to migrate better a more detailed velocity model than an average model is preferred. The velocity model we use is based mainly on a simplification of the results of Iwasaki *et al.* (1994) obtained for the Sognefjord region between our two profiles (see Fig. 1). Their velocity model is well constrained by both *P* and *S* wide-angle reflections and refractions and basically outlines a two-layered crust with an interface at *ca*. 20 km depth. We base our velocity model on the results for the eastern part of their profile, where the crust is thickest and most representative for the midpoints of our two profiles. The crustal model used has constant V_P and σ of 6.30 km s^{-1} and 0.26, respectively, down to 20 km. The lower crustal layer from 20 km and down to Moho has corresponding V_P and σ values of 6.85 km s^{-1} and 0.27, respectively. Below Moho we use the mantle part of the IASP91 velocity model (Kennett & Engdahl 1991).

4.3 Sensitivity analysis of Moho depths

We estimate the sensitivity of Moho depths obtained in the depth migration to the V_P assumptions by performing the migration for three models: the chosen V_P migration model V_{mig} and this model perturbed by ± 3 per cent. σ remains unperturbed. These three V_P models are illustrated in Fig. 3(a). We interpret the structures for depth migration using each of these velocity models. The interpretations for the ± 3 per cent perturbations of V_{mig} are superimposed on the results of the depth migration using the unperturbed model (V_{mig}). Fig. 3(b) illustrates this procedure on 20 synthetic events generated using the V_P model V_{data} (Fig. 3a) with σ equal to 0.265. The depth estimates using the ± 3 per cent perturbations of V_{mig} are positioned at ± 1 km of the Moho depth obtained with the unperturbed V_{mig}. This sensitivity is representative also for the interpreted Moho depths of the observed data.

Likewise, a ± 3 per cent perturbation of σ keeping V_P unperturbed results in a change of inferred Moho depths of ∓ 1 km (not shown). Note that the sensitivity of the obtained Moho depths to an increase in σ is opposite that to an increase in V_P. For the chosen size of the perturbation (3 per cent), the absolute values of the sensitivities are identical (1 km).

The size of the used perturbation (3 per cent) is chosen such that it is representative for the uncertainty of the crustal average model. Christensen & Mooney (1995) estimated the standard deviation of the global average V_P for all types of continental crust to be 3.3–3.6 per cent, depending on weighting. For the migration model used (V_{mig}) and a Moho at 40 km depth, the interval of the crustal average V_P for an uncertainty of 3 per cent is 6.38–6.77 km s^{-1} and 0.257–0.273 for σ.

For common continental crustal rocks, variations in V_P and σ are not independent. The relationship between V_P and σ for different rock types and tectonic regions has been studied both based on laboratory data (e.g. Sobolev & Babeyko 1994; Christensen 1996) and in global seismological studies (e.g. Zandt & Ammon 1995). Their results show large variations with rock composition, but for crustal materials relevant to an old orogen and shield as in southern Norway, an increase in V_P correlates to some degree with an increase in σ. This is especially the case for the crustal averages of V_P and σ which are important in depth migration for Moho depths.

Because depth migration with a model in which V_P is too high results in over estimation of Moho depths whereas depth migration with a model in which σ is too high results in underestimation of Moho depths, the positive correlation of V_P and σ tends to reduce the resulting sensitivity. Therefore, the sensitivity of Moho depths to the combined uncertainty in V_P and σ remains around ± 1 km. However, also picking the Moho *Ps*-phases contributes to the total interpretational uncertainty which we estimate to be within ± 2 km (*cf.* next section).

For a Moho depth of 40 km (20 km of lower crust) the two-layer velocity model based on Iwasaki *et al.* (1994) yields an average V_P of 6.58 km s^{-1} and an average σ of 0.265. The V_P value is slightly higher than the global average for all types of continental crust of 6.45 km s^{-1} obtained by Christensen & Mooney (1995). The σ value is equal to the global average presented in Christensen (1996) also

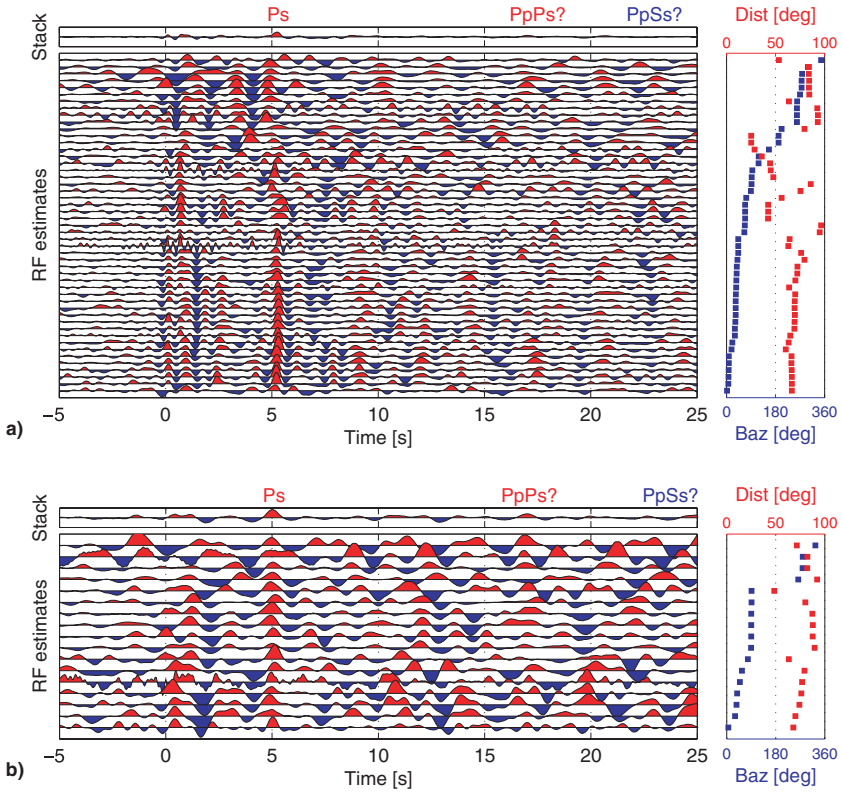

Figure 4. The receiver function estimates for all accepted events recorded by the temporary stations (a) JH03 on the northern profile and (b) BT14 on the southern profile (see Fig. 1). The right-hand side of (a) and (b) shows the distance and the backazimuth (Baz) of each event aligned with the corresponding receiver function estimate. The upper parts of (a) and (b) show the mean (Stack) of all the individual estimates.

for a crustal thickness of 40 km. However, in the migration model used (V_{mig} in Fig. 3a) we extend the lower crust down to 45 km depth (25 km of lower crust) which is deeper than expected for the area. In this way we preclude migrating crustal structures using mantle velocities.

5 RESULTS

5.1 Station examples: JH03 and BT14

As examples of the obtained results, the receiver function estimates for all accepted events at stations JH03 (northern profile) and BT14 (southern profile) are illustrated in Figs 4(a) and (b), respectively. The receiver function estimates for these two stations produce the latest *P*-to-*S* conversions (*Ps*-phases) from Moho obtained for either profile. The *Ps*-phases are clear and arrive at *ca*. 5.2 s for JH03 and at 5.0 s for BT14. The main crustal multiples *PpPs* and *PpSs* are expected at approximately 3.5 and 4.5 times the *Ps* arrival-times, depending on the distance/slowness of the events. The crustal multiples, however, are not as clear as *Ps*. The earliest *Ps*-arrivals observed in this study (not shown) are 3.6 s and 4.0 s obtained for station BT23 (southern profile) and NAO01 (permanent) situated at the west coast and in the Oslo Rift, respectively.

For JH03 the delay-time of the *Ps*-phase from Moho apparently varies with backazimuth. The maximum delay-time of 5.3 s is obtained for arrivals from the northeast (*ca*. 45°) whereas the minimum of 4.8 s occurs for arrivals from southwest to west (*ca*. 225°–270°). This relatively well-resolved 360° periodic variation with backazimuth is not simply explained by the different earthquake distances (i.e. the moveout). It is most likely caused by a Moho dipping to the northeast. The position of station JH03 on Fig. 5, which illustrates the Bouguer gravity anomaly of southern Norway, supports this interpretation. In the vicinity of station JH03, the Bouguer gravity decreases to the northeast with a relatively strong gradient. Forward modelling (not shown) of receiver functions for a dipping Moho using the algorithm of Frederiksen & Bostock (2000) suggests that Moho beneath JH03 dips *ca*. 10° to the northeast.

Azimuthal variation of the Moho *Ps*-phase is also observed at several other stations, for example, JH07, JH09, BT11 and BT23. For these stations the backazimuth coverage is somewhat lower and the *Ps*-arrivals less well defined, and so quantitative modelling of the dip is not possible. Nevertheless, the positions of these stations with indications of a dipping Moho coincide with areas of strong gradients in the Bouguer gravity as should be expected (see Fig. 5).

5.2 The northern profile: Jotunheimen

On Figs 1 and 5 the two dashed lines illustrate the positions of the two profile lines for which the vertical cross-sections of the depth-migrated receiver function estimates are presented. For the northern profile across Jotunheimen, these results and their interpretation are shown in Fig. 6, which also shows the variations of topography and Bouguer gravity anomaly along the profile.

The *Ps*-phase from Moho in Fig. 6 is clear and distinct. It is recognized as the laterally continuous red zone (red is positive amplitude, blue is negative) of varying depth between 30 and 45 km. The depth-scale of the migrated section is relative to sea level. To obtain the crustal thickness, the observed Moho depth and the mean topography must be added.

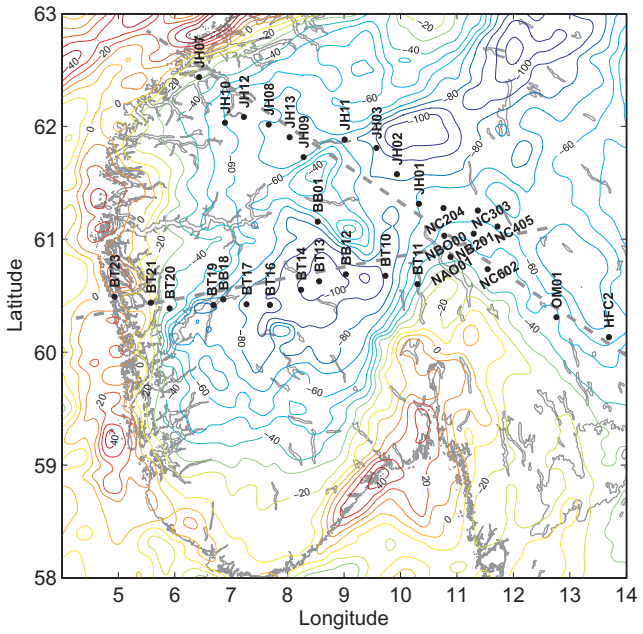

Figure 5. Map of Bouguer gravity anomalies in mGal for the region of southern Norway including positions and names of seismograph stations and the two profile lines. The Bouguer anomalies are contoured at 10 mGal intervals from a grid of 0.1° × 0.2° (Lat × Long). The gridded gravity data were provided by the Danish National Space Center, based on the joint gravity data base for the Nordic Commission of Geodesy, Geoid Project.

The temporary station JH07 is situated at the west end of the profile, about 30 km inland. Beneath this station Moho seems inclined and at a depth of *ca*. 38 km. Moving east along the profile Moho descends to a very well-defined maximum depth of 43 km in the central part below station JH03. Actually the Moho piercing points for this depth are positioned slightly (up to 10 km) to the northeast of station JH03, which itself is offset 25 km northeast from the profile line (see Fig. 1). The minor bulge of Moho from *ca*. 40 km down to 43 km arise from the projection of lateral variations onto the vertical section. This interpretation agrees with the detailed analysis of JH03 in Section 5.1 (*cf.* Fig. 4a) that indicated a Moho dip of *ca*. 10° away from the profile line, descending towards northeast. This is the direction of the adjacent mountain region of Rondane. Moho depths exceeding 43 km are thus expected to occur below the high topography of Rondane (national park with ten summits above 2000 m).

Further east, beneath the permanent stations of NORSAR situated in the northern part of the Oslo Rift (Fig. 1), Moho ascends to a minimum depth of 32 km. Still further east Moho again descends to a depth of 42 km beneath the temporary station OM01, on the Swedish side of the border. At the eastern profile end there is no clear Moho *Ps*-phase in the expected depth range beneath the permanent station HFC2. This result is surprising because of the large number of high-quality events accepted for processing at this station (*cf.* Table 1), which is part of the Hagfors array. A possible explanation could be the position of HFC2 close to the transition from Sweconorwegian tectonic units to the Transscandinavian Igneous Belt (see Fig. 1). Most of the converted (*Ps*) energy from Moho might have been scattered in the transition zone and resulted in the apparently absent Moho. Alternatively, the absent Moho might be explained by a more gradual crust–mantle transition (Moho) in this area.

Beneath the coastward 130 km of the Jotunheimen profile, a westward dipping sub-Moho structure is indicated down to a depth of 5–10 km below Moho. This feature is, however, not as distinct as Moho.

The part of the Jotunheimen profile situated west of the Oslo Rift shows a good correlation between the interpreted depth of Moho and the mean Bouguer gravity. Mean topography and Moho depth correlate also quite well, although the maximum values are offset *ca*. 50 km. Beneath the area with the highest mean topography (>1 km), the Bouguer gravity decreases to *ca*. −75 mGal, and the depth of Moho exceeds 40 km. East of the Oslo Rift no correlation is observed. Instead we observe a rapid increase in Moho depth with no significant changes in either topography or Bouguer gravity.

A local rise in the Bouguer gravity of about 25 mGal is observed for stations JH09 and JH11 (see Fig. 6). Fig. 5 shows that this rise is caused by the northeastern flank of a localized positive gravity anomaly related to the high density rocks of the Jotun Nappe Complex within the Caledonian Allochtons. Outcropping pyroxene-granulites correlate with both gravity and magnetic anomalies. The positive gravity anomaly originates from the upper crust (Smithson *et al.* 1974; Skilbrei 1990), which is consistent with its short wavelength appearance. The receiver function estimates for JH09 and JH11 do not pierce this local nappe complex and the Moho depths obtained correlate well with the level of the regional gravity in this area.

5.3 The southern profile: Hardangervidda

For the southern profile across Hardangervidda, the projected results of the depth migration are shown in Fig. 7 along with the topography and Bouguer gravity variations along the profile line. At the western end of the profile, station BT23 is situated directly at the Atlantic coast. The obtained *Ps* delay-time for Moho is *ca*. 3.6 s, resulting in a Moho depth of 29 km, the overall minimum of our study. Moving east along the profile Moho descends to 38 km beneath station BT19. From station BT19 over BB18 to BT17, an apparent Moho-offset of *ca*. 5 km is observed. Proceeding eastwards Moho descends to 41 km below stations BT13 and BT14, the maximum depth obtained for the southern profile. Further east Moho ascends to 32 km below permanent station NAO01 situated in the Oslo Rift. East of the Oslo Rift the depth of Moho obtained for permanent station NC405 is 39 km although the topography is quite low.

Apparently a Moho offset or at least local Moho topography is resolved beneath stations BT19, BB18 and BT17. Deep high-resolution seismic reflection profiling in the Baltic Shield and elsewhere have resolved Moho steps or local Moho topography of 5–10 km interpreted to reflect ancient crust forming processes. In particular, subduction and collision tectonics may generate local topography on Moho which may survive for a very long time (e.g. BABEL Working Group 1990; Cook *et al.* 1999; Balling 2000). Perhaps the observed Moho topography reflects such remnants of a deep collision tectonic event. Several possibilities exist ranging in age from Gothian over Sveconorwegian to Caledonian. We also note that the stations in question are in the area of the Hardangerfjord where Caledonian (post-compressional) extension structures are observed as crustal-scale shear zones with a vertical throw of about 5 km (Fossen & Hurich 2005). The observed local Moho topography, may also be related to such deep shear zones.

The obtained depths of Moho and the mean Bouguer gravity correlate very well for the part of the profile west of the Oslo Rift

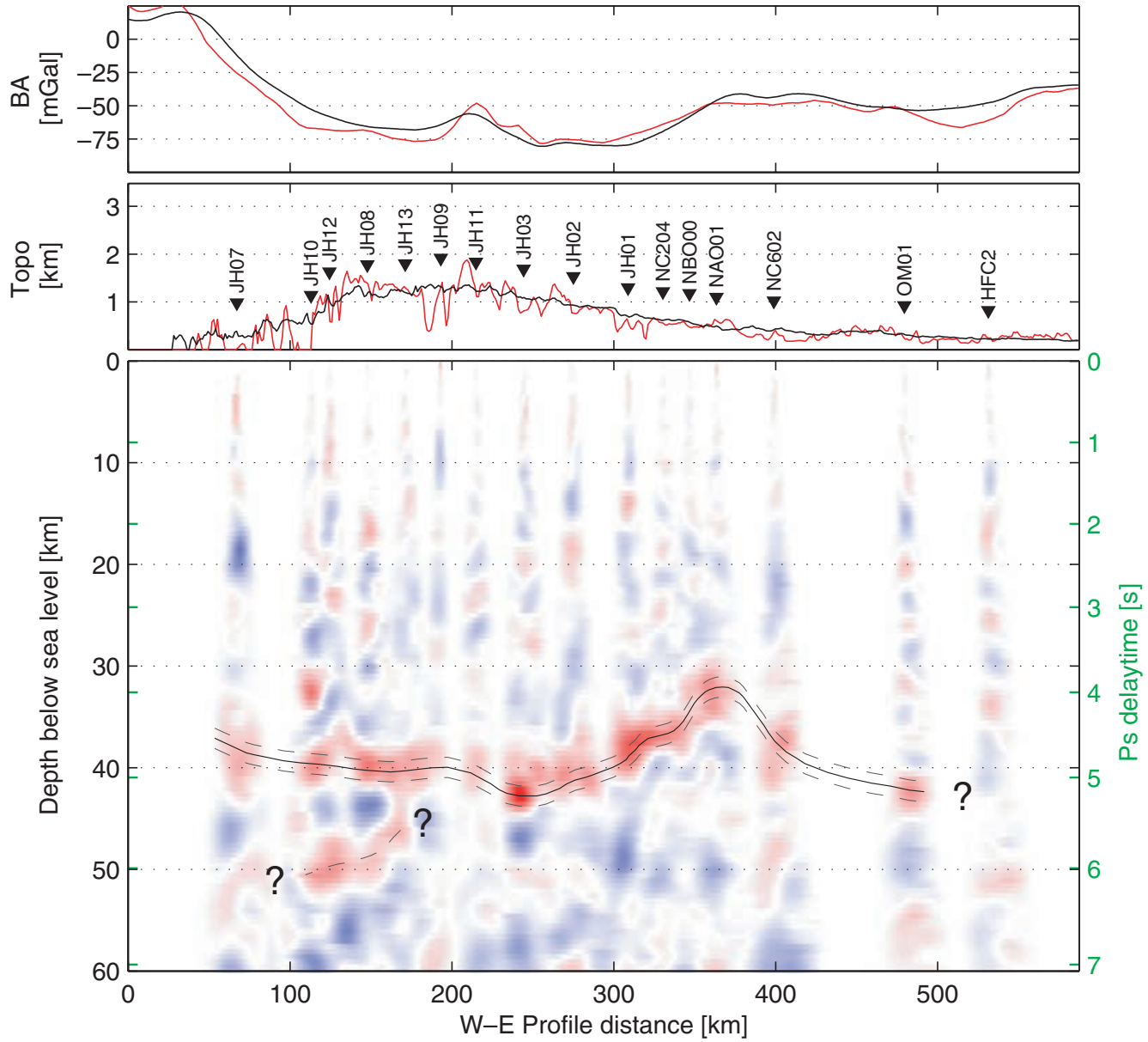

Figure 6. The depth-migrated receiver function estimates for the northern (Jotunheimen) profile projected onto a vertical cross-section through the northern profile line (see Fig. 1). The interpreted Moho is outlined as the full black curve. The two dashed grey curves 1 km above and below the interpreted Moho, respectively, represent the likely uncertainty due to the partly coupled uncertainty in V_P and σ used in the migration model (Sections 4.2 and 4.3). On the right-hand side, in green, is shown an equivalent receiver function timescale (*Ps* delay-time) for a reference slowness of 6.4 s deg^{-1}. Note that time intervals are stretched at depth because of increased velocity. Above the cross-section are shown variations of topography and the Bouguer gravity anomaly (BA) along the profile. Red curves illustrate variations exactly along the profile line and black curves variations of mean values for an interval of ±80 km perpendicular to profile line. Both gravity and topography data are interpolated from a 0.1° × 0.2° grid (Lat × Long).

(*cf.* Fig. 7). This correlation is even closer than that observed for the northern profile, but again the maximum of the mean topography is slightly offset (*ca*. 50 km) to the west as compared to the maximum Moho depth. In general, however, the mean topography and the depth of Moho correlate well.

For station BT23 at the west coast, both the Bouguer gravity and the mean topography are close to zero for the obtained Moho depth of 29 km. The Bouguer gravity minimum of *ca*. −100 mGal coincides with the deepest Moho of 41 km, also situated within less than 50 km of the highest mean topography. These results reveal the presence of a *ca*. 10–12 km thick crustal root beneath the highlands of southern Norway.

Crossing the Oslo Rift from the west to the east the observed correlations apparently cease to exist. An increase in the Moho depth to almost 40 km is observed with no significant change in either topography or Bouguer gravity.

5.4 Comparison to previous studies

Beneath the highlands, centrally on both profiles, the obtained depths of Moho relative to sea level are 4–5 km deeper than previously estimated in the Moho-map of Kinck *et al.* (1993). Their Moho depths were obtained only by interpolation and extrapolation of studies in adjacent areas. These studies are primarily refraction studies from the 1960s and 1970s with the limited recording

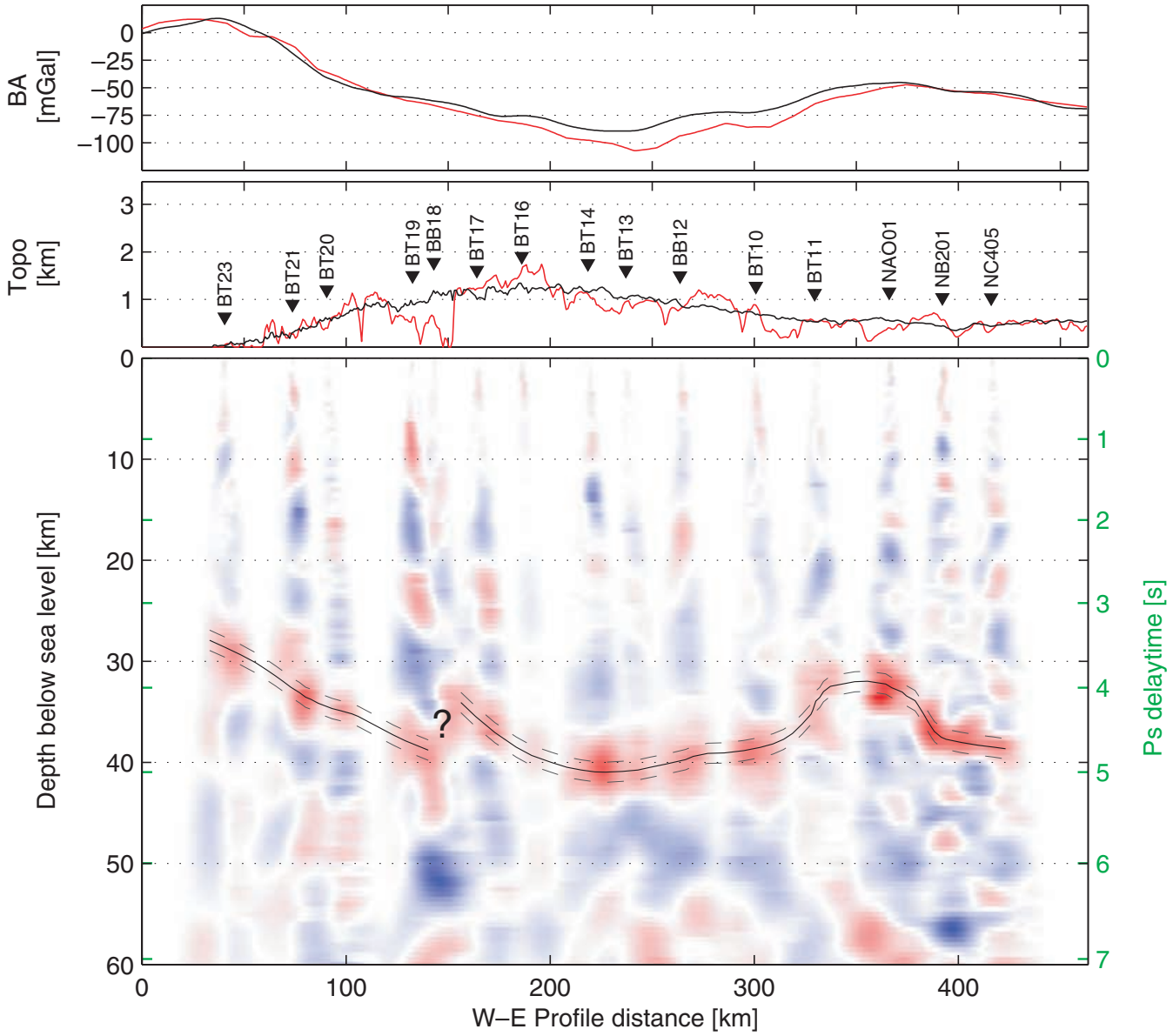

Figure 7. Results of the receiver function depth-migration for the southern (Hardangervidda) profile (see Fig. 1). See caption Fig. 6 for details.

equipment and modelling facilities of that time. In addition, these studies were conducted in adjacent areas with lower topography. This readily explains the apparent differences between our results and the results of Kinck *et al.* (1993).

Ottemöller & Midzi (2003) obtained Moho depths of 38–40 km for station MOL. This result is in very good agreement with the 38 km we obtain for station JH07 situated about 50 km southwest of MOL also in the coastal region. Station BT19 is also situated about 50 km from a permanent station (ODD) for which Ottemöller & Midzi (2003) obtained 34–38 km. For BT19 we obtain a Moho depth of 38 km. For the permanent NORSAR station NAO01, Ottemöller & Midzi (2003) obtain a Moho depth of 34–36 km compared to our value of 32 km which is in excellent agreement with the refraction seismic result (also 32 km) obtained by Kanestrøm (1973) for NAO01.

Between the northern and the southern profile lies the Sognefjord. Both Ottemöller & Midzi (2003) (permanent stations FOO and SUE) and Iwasaki *et al.* (1994) (OBS refraction profile) obtain Moho depths in the range of 30–36 km for this region, shallowest to the west. Inland these results are somewhat shallower than the Moho depths we observe for the two profiles less than 100 km to the north and south. This is, however, to be expected because the gradient of the Bouguer gravity along the Sognefjord is generally lower than that along the corresponding parts of our two profiles (Fig. 5). The slightly elevated Moho observed along the Sognefjord might be caused by the significant erosional unloading and resulting uplift related to the formation of this major fjord-system.

For station BB01 (not included in the migrated sections) situated about 50 km east of the Sognefjord, in an area of high mean topography (*cf.* Fig. 1), the obtained Moho depth is *ca*. 41 km.

One of the seven NORSAR stations (NC303) is not included in either of the two migrated profiles. The obtained Moho depth for NC303 is 38 km, and this result as well as the Moho depths obtained

for the NORSAR stations in general agree well with the previous results of Kanestrøm (1973), Aki *et al.* (1977), Berteussen (1977), Kosarev *et al.* (1987) and Bischoff *et al.* (2004).

6 DISCUSSION AND CONCLUSIONS

In most of the areas investigated the depth of Moho has previously been estimated only by interpolation and extrapolation from studies in adjacent regions (Kinck *et al.* 1993). By receiver function estimation and depth migration we have obtained new, localized and accurate estimates of the depth to Moho beneath two areas of high topography in southern Norway. The sensitivity of Moho depth estimates to realistic deviations from the crustal V_P and σ model used in the depth migration is estimated to be ± 1 km. Including also interpretational uncertainty for the *Ps*-phase, the resulting accuracy of Moho depths is generally within ± 2 km.

Beneath the highlands of Hardangervidda and Jotunheimen, situated in a region strongly influenced by the Caledonian orogeny, our results show that the high mean topography is reflected in increased depth of Moho, a crustal root. The maximum depth obtained is 43 km, but here Moho dips *ca*. 10° to the northeast (*cf.* Section 5.1), indicating that even deeper Moho is expected in this direction which is below the high topography of the Rondane national park. In the Oslo Rift, on the other hand, the crust is significantly thinned, and we obtain Moho depths down to 32 km. East of the Oslo Rift, in Sweden, the crust thickens to more than 40 km, although the mean topography is low. The minimum depth of Moho is 29 km observed in the west at the Atlantic coast.

West of the Oslo Rift both profiles reveal a deep Moho that correlates very well with low mean Bouguer gravity and quite well with high mean topography. The maximum of the mean topography is on both profiles slightly offset to the west (*ca*. 50 km) possibly indicating flexural strength of the crust. East of the Oslo Rift no correlations are observed. Instead, the rapidly increasing Moho depth is not reflected in the corresponding topography and Bouguer gravity. This change is likely to be caused by higher lower-crustal densities in the central parts of the Baltic shield (Henkel *et al.* 1990). From west to east of the Oslo Rift, the disappearance of the correlations represents a transition from a region dominated by Airy-type isostasy to a region where lateral density variations in the lower crust (Pratt-like isostasy) increase in importance.

Below the western part of the northern profile we observe a westward dipping feature just below Moho. In an equivalent position on the southern profile a Moho offset of *ca*. 5 km is apparently resolved. These features could be deep remnants of the long geological history of active tectonics in southern Norway.

In relation to the three proposed mechanisms of Cenozoic uplift mentioned previously, our results have some interesting implications. Regarding magmatic underplating we note that we do not see a clear and continuous conversion above Moho, which indicates that a crustal underplate is either absent or has a rather low velocity, close to that of the pre-intrusion lower crust. If we associate the body between Moho and the westward dipping sub-Moho structure (northern profile) with underplating, then the buoyancy is not in a proper position to support the topography and explain the Bouguer gravity low (see Fig. 5). Hence, our results weaken the hypothesis of magmatic underplating as a cause of Cenozoic uplift. Furthermore, no onshore surface expressions of Cenozoic magmatic activity are observed. Also the hypothesis of a Cenozoic asthenospheric diapir is weakened indirectly. Because the observed crustal root underneath the highlands explains nicely the present topography and the Bouguer gravity, there is little room for extra transient buoyancy in a mantle diapir. Cenozoic lithospheric delamination represents the loss of deep negative buoyancy followed by erosion and differential uplift, which in principle might yield the present topography. However, this hypothesis remains *ad hoc* until more direct geophysical evidence on the deeper mantle structure is gained.

In conclusion, the results we obtain emphasize the contribution to Airy-type isostatic compensation from the *ca*. 10 to 12 km thick present-day crustal root beneath the highlands of southern Norway. The observed crustal root leaves little room for additional buoyancy-effects below Moho. Thus, our observations do not seem consistent with the mechanisms of substantial buoyancy presently suggested to explain a significant (>1 km) Cenozoic uplift widely believed to be the cause of the high topography in present-day southern Norway.

ACKNOWLEDGMENTS

The authors would like to thank Søren Bom Nielsen, Anna Bondo (both University of Aarhus) and Winfried Hanka (GFZ-Potsdam) for valuable support. We also thank FOI (Swedish Research Defence Academy) for availability of the Hagfors data and the University of Uppsala for the loan of 5 mobile seismograph stations used in a pilot study. The constructive reviews by Richard England (University of Leicester) and an anonymous referee are highly appreciated.

This project was financially supported by the Danish Natural Science Research Council.

REFERENCES

Aki, K., Christofferson, A. & Husebye, E.S., 1977. Determination of the three-dimensional seismic structure of the lithosphere, *J. geophys. Res.,* **82**, 277–296.

Al-Damegh, K., Sandvol, E. & Barazangi, M., 2005. Crustal structure of the Arabian Plate: new constraints from the analysis of teleseismic receiver functions, *Earth planet. Sci. Lett.,* **231**, 177–196.

BABEL Working Group, 1990. Evidence for early Proterozoic plate tectonics from seismic reflection profiles in the Baltic Shield, *Nature,* **348**, 34–38.

Balling, N., 1980. The land uplift in Fennoscandia, gravity field anomalies and isostasy, in *Earth Rheology, Isostasy and Eustasy*, pp. 297–321, ed. Mörner, N.-A., John Wiley & Sons, New York.

Balling, N., 1984. Gravity and isostasy in the Baltic Shield, in *First EGT Workshop: The Northern Segment*, pp. 53–68, eds Galson, D.A. & Mueller, S., European Science Foundation, Strassbourg.

Balling, N., 2000. Deep seismic reflection evidence for ancient subduction and collision zones within the continental lithosphere of northwestern Europe, *Tectonophysics,* **329**, 269–300.

Berteussen, K.A., 1977. Moho depth determinations based on spectral-ratio analysis of NORSAR long-period P waves, *Phys. Earth planet. Inter.,* **15**, 13–27.

Bischoff, M., Schweitzer, J. & Meier, T., 2004. Comparison of the Love-Rayleigh discrepancy in central Europe (GRSN) and southern Scandinavia (NORSAR), Semiannual Technical Summary 2, NORSAR.

Bostock, M.G., 1998. Mantle stratigraphy and evolution of the Slave province, *J. geophys. Res.,* **103**, 21 183–21 200.

Bostock, M.G., Hyndman, R.D., Rondenay, S. & Peacock, S.M., 2002. An inverted continental Moho and serpentinization of the forearc mantle, *Nature,* **417**, 536–538.

Christensen, N.I., 1996. Poisson's ratio and crustal seismology, *J. geophys. Res.,* **101**, 3139–3156.

Christensen, N.I. & Mooney, W.D., 1995. Seismic velocity structure and composition of the continental crust: a global view, *J. geophys. Res.,* **100**, 9761–9788.

Cook, F.A., Velden, A., Hall, K.W. & Roberts, B., 1999. Frozen subduction in Canadas Northwest Territories: lithoprobe deep lithospheric reflection profiling of the western Canadian Shield, *Tectonics,* **18**, 1–24.

Dahl-Jensen, T. *et al.*, 2003. Depth to Moho in Greenland: receiver-function analysis suggests two Proterozoic blocks in Greenland, *Earth planet. Sci. Lett.,* **205**, 379–393.

Doré, G.A., 1992. The base tertiary surface of southern Norway and the northern North Sea, *Norwegian J. Geol.,* **72**, 259–265.

Ebbing, J. & Olesen, O., 2005. The Northern and Southern Scandes-structural differences revealed by an analysis of gravity anomalies, the geoid and regional isostasy, *Tectonophysics,* **411**, 73–87.

Fossen, H. & Hurich, C.A., 2005. The Hardangerfjord Shear Zone in SW Norway and the North Sea: a large-scale low-angle shear zone in the Caledonian crust, *J. Geol. Soc.,* **162**, 675–687.

Frederiksen, A.W. & Bostock, M.G., 2000. Modelling teleseismic waves in dipping and anisotropic structures, *Geophys. J. Int.,* **141**, 401–412.

Gabrielsen, R.H., Braathen, A., Olesen, O., Faleide, J.I., Kyrkjebø, R. & Redfield, T., 2005. Vertical movements in south-western Fennoscandia: a discussion of regions and processes from the present to the Devonian, in *Onshore-Offshore Relationships on the North Atlantic Margin. Norwegian Petroleum Society (NPF) Special Publication 12*, pp. 1–28, eds Wandås, B., Eide, E., Grandstein, F. & Nystuen, J., Elsevier, Amsterdam.

Gaál, G. & Gorbatschev, R., 1987. An outline of the Precambrian evolution of the Baltic Shield, *Precambrian Res.,* **35**, 15–52.

Gee, D.G. & Sturt, B.A., 1985. *The Caledonide Orogen– Scandinavia and Related Areas*, John Wiley & Sons, Chichester.

Gorbatschev, R. & Bogdanova, S., 1993. Frontiers in the Baltic Shield, *Precambrian Res.,* **64**, 3–21.

Gossler, J., Kind, R., Sobolev, S.V., Kämpf, H., Wylegalla, K., Stiller, M., & TOR Working Group, 1999. Major crustal features between the Harz Mountains and the Baltic Shield derived from receiver functions, *Tectonophysics,* **314**, 321–333.

Henkel, H., Lee, M.K., Lund, C.E. & Rasmussen, T., 1990. An integrated geophysical interpretation of the 2000 km FENNOLORA section of the Baltic Shield, in *The European Geotraverse: Integrative Studies*, pp. 297–321, eds Freeman, R. & Mueller, S., European Science Foundation, Strassbourg.

Iwasaki, T., Sellevoll, M.A., Kanazawa, T., Veggeland, T. & Shimamura, H., 1994. Seismic refraction study along the Sognefjord, south-west Norway, employing ocean-buttom seismometers, *Geophys. J. Int.,* **119**, 791–808.

Japsen, P. & Chalmers, J.A., 2000. Neogene uplift and tectonics around the North Atlantic: overview, *Global planet. Change,* **24**, 165–173.

Kanestrøm, R., 1973. A crust-mantle model for the NORSAR area, *Pure appl. Geophys.,* **105**, 729–740.

Kanestrøm, R. & Haugland, K., 1971. Profile section 3–4, in *Seismic Investigations of the Crust and Upper Mantle in Norway*, pp. 2–17, ed. Vogel, A., Natural Science Research Council, Stockholm.

Kanestrøm, R. & Nedland, S., 1975. Crustal structure of southern Norway. A reinterpretation of the 1965 seismic experiment, Institute report, Seismological Observatory, University of Bergen.

Kennett, B. & Engdahl, E.R., 1991. Traveltimes for global earthquake location and phase identification, *Geophys. J. Int.,* **105**, 429–465.

Kinck, J.J., Husebye, E.S. & Larsson, F.R., 1993. The Moho depth destribution in Fennoscandia and the regional tectonic evolution from Archean to Permian times, *Precambrian Res.,* **64**, 23–51.

Kind, R., Kosarev, G.L. & Petersen, N.V., 1995. Receiver functions at the stations of the German Regional Seismic Network (GRSN), *Geophys. J. Int.,* **121**, 191–202.

Kosarev, G., Kind, R., Sobolev, S.V., Yuan, X., Hanka, W. & Oreshin, S., 1999. Seismic evidence for a detached Indian lithospheric mantle beneath Tibet, *Science,* **283**, 1306–1309.

Kosarev, G.L., Makeyeva, L.I. & Vinnik, L.P., 1987. Inversion of teleseismic P-wave particle motions for crustal structure in Fennoscandia, *Phys. Earth planet. Inter.,* **47**, 11–24.

Langston, C.A., 1979. Structure under Mount Rainier, Washington, inferred from teleseismic body waves, *J. geophys. Res.,* **89**, 4749–4762.

Lidmar-Bergström, K., Ollier, C.D. & Sulebak, J.R., 2000. Landforms and uplift history of southern Norway, *Global planet. Change,* **24**, 211–231.

Mykkeltveit, S., 1980. A seismic profile in southern Norway, *Pure appl. Geophys.,* **118**, 1310–1325.

Nielsen, S.B. *et al.*, 2002. Paleocene initiation of the Cenozoic uplift in Norway, *Geological Society, London, Special publications,* **196**, 45–65.

Ottemöller, L. & Midzi, V., 2003. The crustal structure of Norway from inversion of teleseismic receiver functions, *J. Seism.,* **7**, 35–48.

Owens, T.J., Taylor, S.R. & Zandt, G., 1987. Crustal structure at regional seismic test network stations determined from inversion of broadband teleseimic *P* waveforms, *Bull. seism. Soc. Am.,* **77**, 631–662.

Petersen, N., Vinnik, L., Kosarev, G., Kind, R., Oreshin, S. & Stammler, K., 1993. Sharpness of the mantle discontinuities, *Geophys. Res. Lett.,* **20**, 859–862.

Roberts, D., 2003. The Scandinavian Caledonides: event chronology, palaeogeographic setting and likely modern analogues, *Tectonophysics,* **365**, 283–299.

Rohrman, M. & van der Beek, P., 1996. Cenozoic postrift domal uplift of North Atlantic margins: an asthenospheric diapirism model, *Geology,* **24**, 901–904.

Sellevoll, M.A. & Warrick, R.E., 1971. A refraction study of the crustal structure in southern Norway, *Bull. seism. Soc. Am.,* **61**, 457–471.

Skilbrei, J.R., 1990. Structure of the Jotun Nappe Complex, southern Norwegian Caledonides: ambiguity of gravity modelling and reinterpretation, Report, Geological Survey of Norway.

Smithson, S.B., Ramberg, I.B. & Grønlie, G., 1974. Gravity interpretation of the Jotun Nappe of the Norwegian Caledonides, *Tectonophysics,* **22**, 205–222.

Sobolev, S.V. & Babeyko, A.Y., 1994. Modeling of mineralogical composition, density and elastic wave velocities in anhydrous magmatic rocks, *Surveys in Geophysics,* **15**, 515–544.

Stuevold, L.M. & Eldholm, O., 1996. Cenozoic uplift of Fennoscandia inferred from a study of the mid-Norwegian margin, *Global planet. Change,* **12**, 359–386.

Svenningsen, L. & Jacobsen, B.H., 2004. Comment on 'Improved inversion for seismic structure using transformed, S-wavevector receiver functions: Removing the effect of the free surface' by Anya Reading, Brian Kennett, and Malcolm Sambridge, *Geophys. Res. Lett.,* **31**, 1–2.

Torsvik, T.H., 1998. Palaeozoic palaeogeography: a North Atlantic viewpoint, *Geol. Fören. Stockholm Förhandl.,* **120**, 109–118.

Torsvik, T.H. & Cocks, L.R.M., 2005. Norway in space and time: a Centennial cavalcade, *Norwegian J. Geol.,* **85**, 73–86.

Vinnik, L.P., 1977. Detection of waves converted from P to SV in the mantle, *Phys. Earth planet. Inter.,* **15**, 39–45.

Windley, B., 1992. Precambrian Europe, in *A Continent Revealed: the European Geotraverse*, pp. 139–152, eds Blundell, D., Freeman, R. & Mueller, S., Cambridge University Press, Cambridge.

Zandt, G. & Ammon, C.J., 1995. Continental crust composition constrained by measurements of crustal Poisson's ratio, *Nature,* **374**, 152–154.

Zhu, L. & Kanamori, H., 2000. Moho depth variation in southern California from teleseismic receiver functions, *J. geophys. Res.,* **105**, 2969–2980.